Observations of low-frequency electromagnetic plasma waves upstream from the Martian shock

D. A. Brain,[1] F. Bagenal,[1] M. H. Acuña,[2] J. E. P. Connerney,[2] D. H. Crider,[2] C. Mazelle,[3] D. L. Mitchell,[4] and N. F. Ness[5]

Received 7 November 2000; revised 9 July 2001; accepted 9 July 2001; published 15 June 2002.

[1] We have analyzed magnetic field data returned from Mars Global Surveyor (MGS) for signatures of electromagnetic plasma waves upstream from the Martian bow shock. We discuss two recurring wave features in the data. Left-hand polarized waves (0.04–0.10 Hz) observed near the local proton gyrofrequency (PCWs) propagate at small to moderate angles to the magnetic field and have amplitudes that decrease with distance from Mars. They are concentrated in two locations upstream of the Martian shock. PCWs were reported from Phobos 2 observations and can be attributed to solar wind pickup of Mars' hydrogen exosphere. Higher-frequency waves (0.4–2.3 Hz) are observed when MGS is magnetically connected to the Martian shock. These waves have not been reported at Mars before, but have been reported at many solar system bodies, and are attributed to whistler waves generated at the shock and propagating upstream. The sense of polarization (left-handed or right-handed) of the whistler waves observed in the spacecraft frame depends upon the angle between the magnetic field and the solar wind flow direction. The whistler waves at Mars follow the trends in frequency, amplitude, propagation angle, and eccentricity observed at other solar system bodies. *INDEX TERMS:* 6225 Planetology: Solar System Objects: Mars; 2772 Magnetospheric Physics: Plasma waves and instabilities; 2154 Interplanetary Physics: Planetary bow shocks; *KEYWORDS:* Mars, MGS, upstream, waves, electromagnetic

1. Introduction

[2] One observational result of Mars missions has been the detection of electromagnetic waves and disturbances upstream from the Martian shock [e.g., *Riedler et al.*, 1989; *Grard et al.*, 1989; *Russell et al.*, 1990; *Sagdeev et al.*, 1990; *Barabash and Lundin*, 1993]. The newest and largest set of observations of upstream waves have been made by the magnetometer/electron reflectometer (MAG/ER) on board Mars Global Surveyor (MGS). Perturbations to the magnetic field have been observed throughout the Martian system by MGS, which has more complete coverage of the solar wind interaction in solar zenith angle and in altitude than previous spacecraft. Waves are evident in MGS data upstream of the bow shock [*Mazelle et al.*, 2000; *Brain et al.*, 1998] and in the Martian sheath [*Cloutier et al.*, 1999; *Crider*, 1999]. Here we focus on two waves repeatedly observed in MGS MAG data outside of the Martian bow shock. One wave (0.04–0.10 Hz) is observed at the local proton gyrofrequency and is associated with pickup of Mars' neutral hydrogen exosphere. The other wave is seen at higher frequencies (0.4–2.3 Hz) and has been identified at other solar system bodies as a whistler wave.

[3] Waves at the proton gyrofrequency (PCWs) have been previously detected at Mars by *Russell et al.* [1990]. Using three orbits of high time resolution data from the MAGMA magnetometer on Phobos, the amplitude, eccentricity, polarization, and propagation angle were reported for four examples of PCWs. It was noted that the waves had very low amplitudes ($\sim$0.15 nT, $\Delta B/B \sim .06$), are left-hand elliptically polarized, and propagate at small to moderate angles relative to the magnetic field. Wave observations near the shock were complicated by shock-related turbulence, and waves were not observed further upstream than 2–3 R_M from Mars. From the frequency, location, polarization, and propagation of the waves *Russell et al.* [1990] concluded that the waves formed by ionization of Mars' hydrogen exosphere upstream of the shock. This conclusion was bolstered and extended by results from the Automatic Space Plasma Experiment with Rotating Analyzer (ASPERA), which observed ring distributions of pickup protons from Mars' extended hydrogen corona and derived altitude profiles of pickup proton fluxes and exospheric number densities using the observed energy in the ring distributions [*Barabash et al.*, 1991]; the cyclotron instability of the protons would produce Alfvèn waves observed by the magnetometer. There is no evidence at Venus for left-hand polarized proton cyclotron waves analogous to the Martian waves [*Russell et al.*, 1992], suggesting that Martian waves near the proton cyclotron frequency

[1]Laboratory for Atmospheric and Space Physics, University of Colorado, Boulder, Colorado, USA.
[2]NASA Goddard Space Flight Center, Greenbelt, Maryland, USA.
[3]Centre d'Etude Spatiale des Rayonnements, Toulouse, France.
[4]Space Sciences Laboratory, University of California, Berkeley, California, USA.
[5]Bartol Research Institute, University of Delaware, Newark, Delaware, USA.

0148-0227/02/2000JA000416$09.00

form because the Martian exosphere extends beyond the Martian bow shock, unlike the case at Venus. The pickup mechanism has been studied extensively in the case of comets [e.g., *Mazelle and Neubauer*, 1993; *Brinca*, 1991; *Tsurutani*, 1991; *Gary*, 1991; and references therein]. Recently, *Sauer et al.* [2001] have shown that pickup protons at Mars are capable of exciting nonlinear coherent waves at the local proton gyrofrequency.

[4] Upstream whistler waves have been reported for many solar system bodies, but never for Mars. These waves (sometimes called "1 Hz waves") were first observed at Earth in the shock foot by *Heppner et al.* [1967] and were first noted upstream from the shock by *Russell et al.* [1971]. *Fairfield* [1974] identified these waves as whistlers. Subsequently, whistlers have been reported upstream from other solar system bodies, including Venus, Mercury, and Saturn [*Orlowski et al.*, 1990; *Orlowski et al.*, 1992]. In general, the waves are observed at frequencies greater than the local proton gyrofrequency. They propagate obliquely to the magnetic field and appear very soon after the spacecraft passes onto field lines connected to the bow shock. When observed in the inner solar system, the waves are usually left-hand elliptically polarized, but are observed as right-hand polarized waves when they propagate at a large angle to the solar wind velocity. The percentage of waves with right-hand polarization increases with the heliocentric distance of the solar system body around which the waves are being observed. The amplitude of the waves decreases with distance (measured along the magnetic field line) from the shock. Early studies of upstream whistlers at Earth favored a local generation mechanism in the foreshock because of their association with ion beams [*Hoppe et al.*, 1981], but subsequent work showed that ion beams are not always observed in conjunction with these waves [*Hoppe et al.*, 1982], and suggested that the whistlers are generated at the shock and propagate upstream [*Orlowski et al.*, 1995]. Upstream propagation is possible because the whistler group velocity is greater than the solar wind velocity; the waves propagate upstream faster than they are convected downstream. A wide variety of scenarios have been proposed as the generation mechanism [*Wong and Smith*, 1994], including reflected solar wind electrons from the shock ramp [*Sentman et al.*, 1983], cross-field drift at the shock [*Orlowski et al.*, 1995], shock front perturbations [*Baumgärtel and Sauer*, 1995], reflected protons which gyrate back to the shock [*Hellinger and Mangeney*, 1997], and electron temperature anisotropies (for nearly field-aligned whistlers) [*Mace*, 1998]. Similarities between the wave characteristics at each body suggest that similar processes are responsible for the waves throughout the solar system, and that the size and shape of the shock do not play significant roles in the generation or subsequent damping of the waves [*Orlowski and Russell*, 1995]. Mars represents an additional data point for understanding of these whistler waves.

[5] Here we present observations by MGS MAG of plasma waves outside of the Martian bow shock. Observations of waves at the local proton gyrofrequency confirm previous observations from the Phobos spacecraft. We further discuss the characteristics and spatial distribution of these waves on the basis of data from over 500 MGS orbits. Upstream whistler waves are reported from magnetometer data for the first time at Mars, and their characteristics are placed in context with observations from other solar system bodies. We discuss the observations and analyses necessary for determination of the generation mechanism of each wave.

2. Observations

[6] The MAG instrument consists of two triaxial fluxgate magnetometers mounted on the ends of the spacecraft solar panels [*Acuña et al.*, 1998]. Vector measurements of magnetic field are made at a rate of up to 32 samples per second at a resolution of up to 0.005 nT per axis. At a given sample rate (32, 16, or 8 samples per second), MAG records the full value of the magnetic field every 24th sample, and only records the change in magnetic field from one sample to the next for the remaining samples. Our analysis includes high time resolution observations (using all samples) and low time resolution observations (using only samples where the full magnetic field value is recorded). With a Nyquist frequency ranging from 0.17–0.67 Hz, low time resolution observations are adequate for study of waves at the proton gyrofrequency for typical upstream magnetic field strengths. High time resolution data (with minimum Nyquist frequency of 4 Hz) are required for analysis of the whistler waves.

[7] The position of the magnetometers on the spacecraft solar panels creates a unique set of calibration issues, which are discussed by *Acuña et al.* [2001]. The data have been calibrated to include dynamic and static magnetic field contributions from the MGS spacecraft and solar panels, with accuracy of $\sim$0.5 nT in Mars' shadow and $\sim$1 nT elsewhere. The main remaining MGS contribution to magnetic field measurements comes from the thermal response of the solar panels, which heat up as they are exposed to sunlight. This response generally occurs at a frequency much lower than the frequency of either wave feature discussed here. Thus, with proper filtering of the data we can obtain a reliable signature of the magnetic field perturbation due to each wave. However, the direction of the ambient magnetic field is uncertain to within the accuracy of the calibration. Spacecraft calibration is available for low time resolution data, which we use to study the waves at the cyclotron frequency. Because of the time resolution of spacecraft and solar panel engineering data the calibration is not available for high time resolution data. We use high pass filtered high time resolution data (which does not include the spacecraft calibration) to study the whistler waves, and we use the corresponding low time resolution data to estimate the background field direction.

[8] The orbit geometry of the MGS mission during each of its phases is described by *Albee* [2000]. The premapping portion of the mission is divided into four phases. Three of these mission phases have an elliptical orbit geometry that took MGS outside of the Martian shock, enabling observation of upstream waves. The orbit geometry for each of these mission phases is shown in Figure 1. The first aerobraking mission phase (AB1) occurred immediately after orbit insertion and lasted from 13 September 1997, through 25 March 1998, lasting 198 orbits. The spacecraft orbit evolved considerably in this time, and includes observations at middle to high solar zenith angles and at large

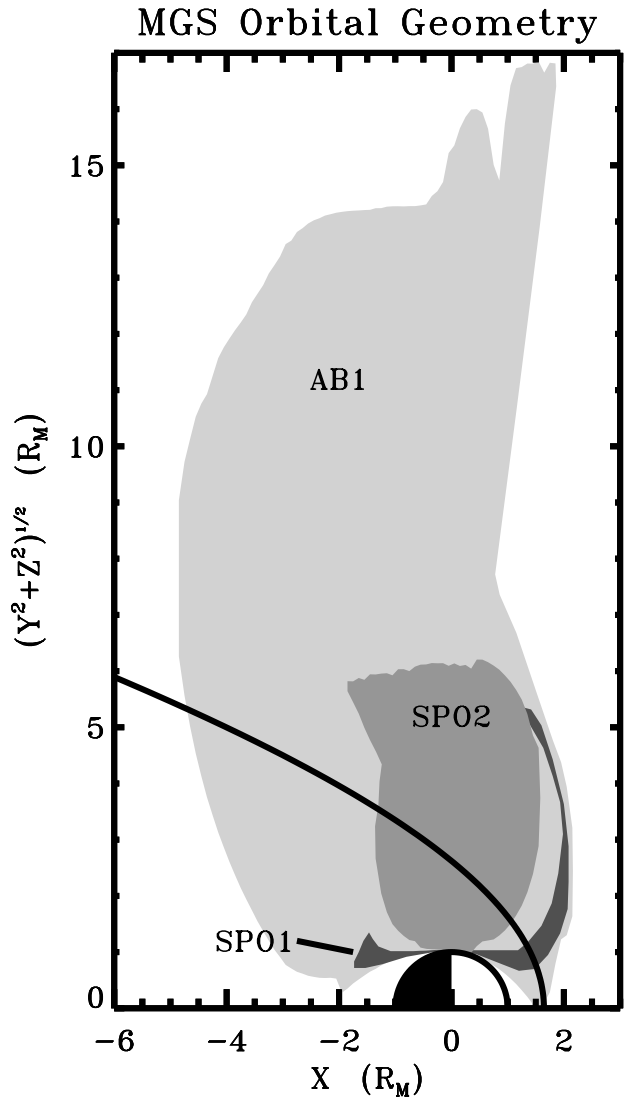

Figure 1. Mars Global Surveyor (MGS) orbit geometry for three premapping mission phases in sun-state cylindrical coordinates. The best fit bow shock [from *Vignes et al.*, 2000] is shown in black.

distances from Mars. The first Science Phasing Orbit mission phase (SPO1) occurred from 26 March 1998, through 27 May 1998. At low to moderate solar zenith angles, 130 orbits yielded a large number of upstream observations over a limited region of space relative to Mars and the Sun. The SPO2 mission phase occurred from 28 May 1998, through 23 September 1998, and lasted 245 orbits. Observations outside of the shock are closer to the terminator plane than for SPO1 and do not extend to the large distances of AB1.

[9] Three Cartesian coordinate systems were used in the data analysis. Sun-state (SS) coordinates are used to reference MGS to Mars. At a given instant in this coordinate system, the Mars-Sun line is taken as the $+x$ axis, the negative of the Martian orbital velocity vector is taken as the $+y$ direction, and a vector upward out of the Martian orbital plane completes the right-handed coordinate system. Mean-field coordinates (sometimes called field-aligned coordinates) are useful for studying wave properties relative to the ambient solar wind magnetic field direction. In this coordinate system the mean magnetic field over a period of time long enough to encompass many cycles of the plasma waves (typically 5 min in this work) is taken as the $+z$ direction, and two vectors perpendicular to the mean-field direction complete the right-handed coordinate system. Finally, principal axis coordinates (PA) are used as the coordinate system of the wave. For an elliptically polarized wave in PA coordinates, the wave propagation vector, **k**, lies in the $\pm z$ direction (the sign of the vector cannot be uniquely determined), and magnetic field oscillations occur in the x-y plane. The x and y axes are defined along the semimajor axes of oscillation. PA coordinates are determined by calculating the plane in which the majority of magnetic field oscillation occurs. A thorough discussion of principal axis analysis as it applies to plasma waves observed in time series magnetic field data is given by *Song and Russell* [1999]. For individual wave observations, the SS, mean-field, and PA coordinate systems are used in conjunction to determine the relationships between wave propagation direction, mean magnetic field direction, and the Martian solar wind interaction.

3. Data Analysis

[10] Wave activity is readily apparent in the magnetic field data. Figure 2 shows 1 min of high time resolution MAG data in SS coordinates from 24 April 1998. Two superposed wave frequencies are identified: one low-frequency component (~13 s period) and one high-frequency component (~1 s period). The lower-frequency wave occurs near the local proton cyclotron frequency; we will show that the high-frequency wave is a whistler wave.

[11] The evolution of the power and frequency of these waves with time can be studied by creating dynamic fast Fourier spectra from MAG data. The data were rotated into mean-field coordinates and high-pass filtered to remove the solar panel thermal contribution and other long-period fluctuations not associated with the wave oscillations identified in the raw data. Windowed fast Fourier transforms (FFTs) of 150 s of data (sufficient to capture multiple periods of the cyclotron wave) were taken every 30 s. The resultant power from each FFT is shown for the $+x$ mean-field magnetic field component as a spectrogram in Figure 3. The orbit shown is a SPO1 orbit. Data gaps between 1910 and 1940 UT are apparent in the spectrum. Beneath the bow shock (time < 1900 UT) it is difficult to pick out any specific wave features. The FFT technique does not work well because the background magnetic field and plasma environment in the magnetosheath change rapidly over each 150 s span of data. The analysis of waves downstream of the shock is beyond the scope and techniques of this work, but it is a subject for study during future work. Outside of the shock (time > 1900 UT) the technique works well, and we can see the two wave modes clearly. The low-frequency wave is long-lived and occurs at a frequency that is indistinguishable from the local proton cyclotron frequency (denoted by the black line in the spectrum). At times (1950–2070 UT) the wave is accompanied by a lower-frequency signal. The low-frequency "companion" feature is sometimes seen in data from other orbits, and it is characteristic of the coherent wave generation mechanism proposed by *Sauer et al.* [2001] under specific conditions

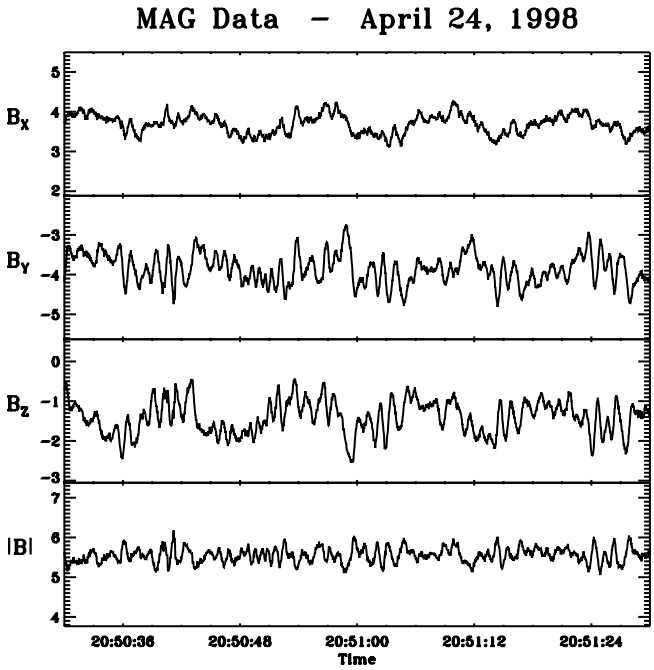

Figure 2. High time resolution magnetometer (MAG) data in sun-state (SS) coordinates from 24 April 1998. MGS is $\sim$2.9 R_M outside of the Martian shock, at solar zenith angle of $\sim$65°. Two wave modes are evident with periods of $\sim$13 s and $\sim$1 s.

(e.g., relative drift of the pickup ion population). The high-frequency feature occurs intermittently for this orbit. Waves near 1 Hz are evident close to the bow shock (1920–2020 UT), and again further upstream (2070–2200 UT). The characteristics of both wave features in this orbit are representative of the wave features during other orbits as well, though the frequency and power of the waves varies from orbit to orbit.

3.1. Low-Frequency Waves

[12] The initial Phobos observations of waves at the local proton cyclotron frequency [*Russell et al.*, 1990, 1992] provide context for our observations. With many more orbits of data and more complete spatial coverage of the region outside of the Martian shock, MGS data are examined to confirm the results from Phobos, and to address the issues of the spatial distribution of the waves, and how PCW characteristics vary with location. Low time resolution MAG data from the AB1, SPO1, and SPO2 mission phases were used for the analysis.

[13] To further investigate the PCW characteristics, high pass filtered data (cutoff frequency of 0.005 Hz) from each orbit were examined every 30 s. The peak frequency was determined from an FFT of the data at each time. The length of the window for the FFT varied according to the local gyrofrequency. When waves were evident in mean-field time series data at the peak frequency, we used a principal axis analysis to extract the eccentricity, amplitude, polarization, and propagation direction for each identified wave. Figure 4 shows the spatial distribution of wave detections in cylindrical coordinates. At each location the percentage of observations that contained low-frequency waves is indicated in color. The best fit bow shock, determined from MGS data, is shown in red. Two areas outside of the shock contain high concentrations of waves near the gyrofrequency: the most sunward and lowest solar zenith angle locations (sampled during SPO1 and some AB1 orbits), and high solar zenith angle locations (the most tailward AB1 observations). Beneath the shock, few waves were observed on the planetary dayside, most likely because the turbulent nature of the magnetosheath makes detection of the waves

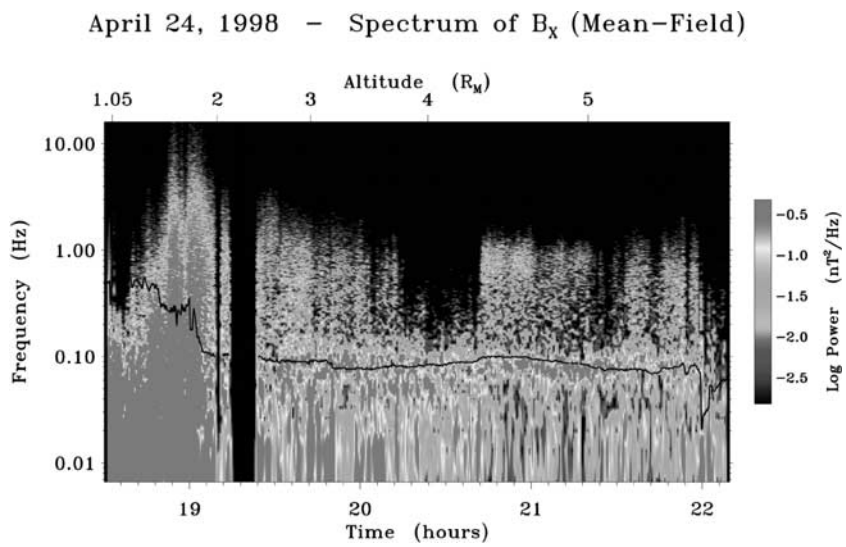

Figure 3. Spectrogram of power as a function of frequency and time for the B_X field component in mean-field coordinates for 24 April 1998. The bow shock crossing occurs at $\sim$1910 UT, after which MGS is outside of the shock for this SPO1 orbit. Low-frequency waves occur near the local proton gyrofrequency (plotted over the spectrogram in black), and high-frequency waves occur near 1 Hz. There are two data gaps between 1906 and 1924 UT. See color version of this figure at back of this issue.

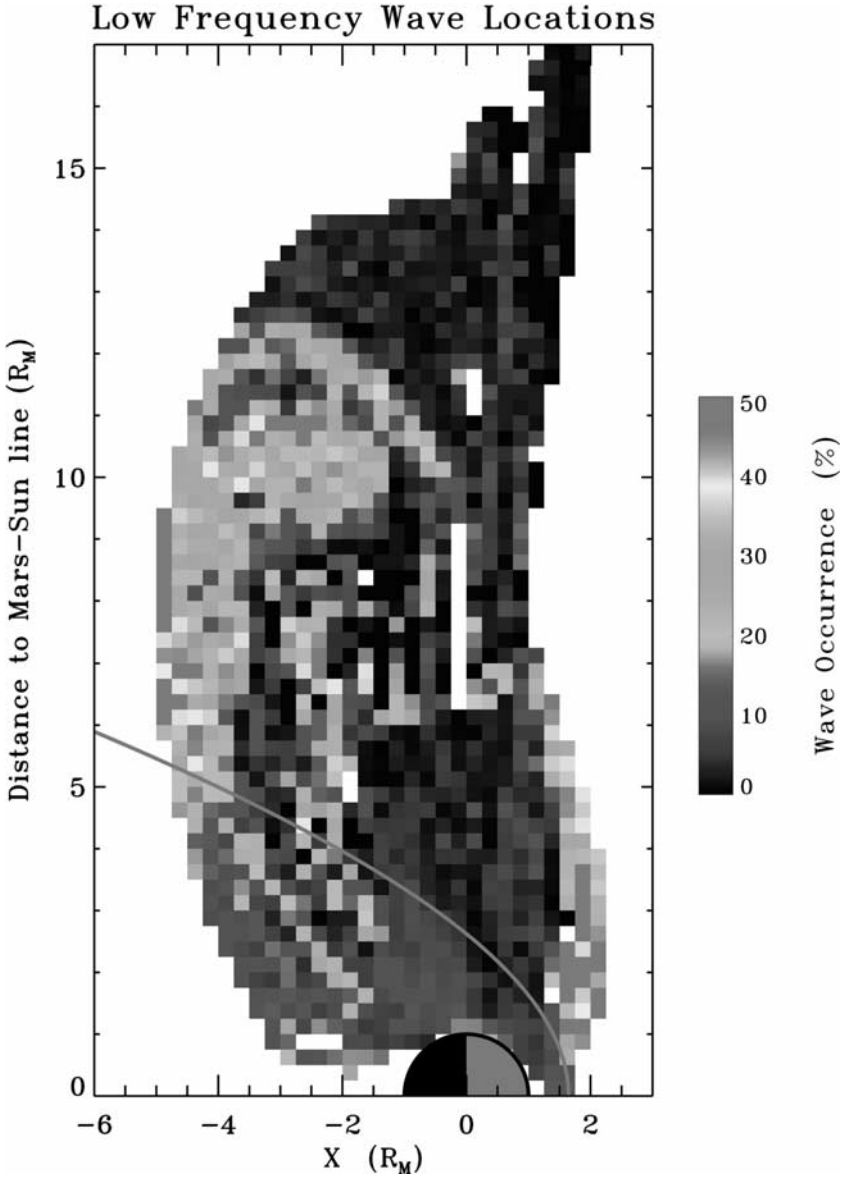

Figure 4. Spatial distribution of waves detected at the local proton gyrofrequency. The percentage of observations that were determined to contain waves is shown for each spatial bin. The best fit bow shock is indicated in red. See color version of this figure at back of this issue.

problematic, as discussed in section 3. However, we were able to detect waves in the nightside magnetosheath.

[14] Principal axis analysis was used to determine the characteristics of each identified wave. The waves typically have more power perpendicular to the mean-field direction then along it, which indicates that **k** makes a small or moderate angle with the mean-field direction. Figure 5a shows power spectra for all three field components in mean-field coordinates on 13 April 1998, from 1630 to 1730 UT. The displayed power spectra were created by averaging 120 FFTs over a 60 min time span. The peak near the average local proton gyrofrequency is very clear, and the power in the mean-field direction is smaller by a factor of $\sim$10 than the power in either of the other two directions. The angle between **k** and the mean-field direction is small ($\theta_{\mathbf{kB}} \sim 20°$). PCWs are always left-hand elliptically polarized. Figure 5b shows a hodogram of 2 min of data in the same time period. The data were band pass filtered between 0.005 Hz and 0.1 Hz. The magnetic field oscillates in a left-hand sense around the propagation vector; the mean-field is out of the page in this instance.

[15] The characteristics of PCWs outside of the shock are summarized in Table 1. The typical frequency range is within 20% of the local proton gyrofrequency, and is consistent with upstream magnetic field strengths of 2.7–6.6 nT. The amplitude of the waves (in nT) is larger than observed by Phobos, as is the amplitude relative to the magnitude of the background field. Both the eccentricity and the angle between the propagation direction and the background field agree with the values reported from Phobos. Table 1 further summarizes PCW observations in the two regions of high wave concentration: the ''subsolar'' low zenith angle waves observed during SPO1, and the ''flank'' high zenith angle waves observed during AB1.

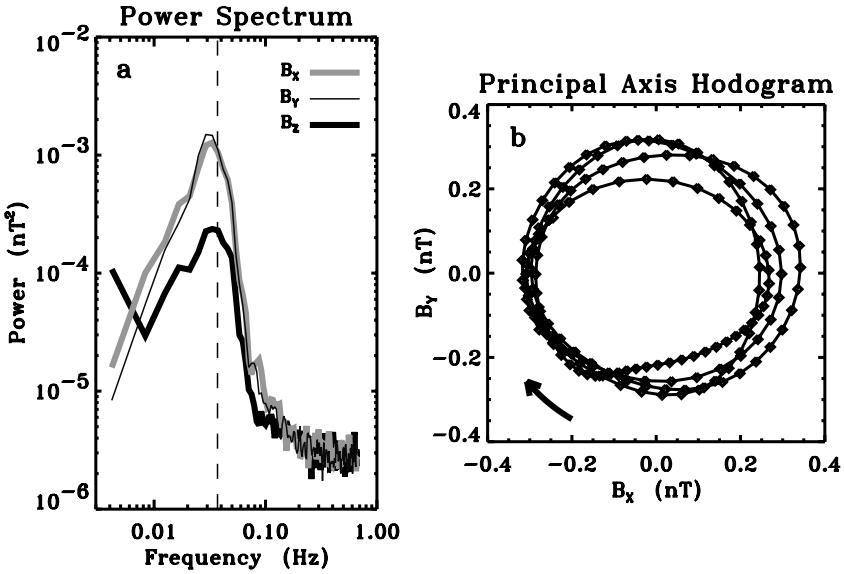

Figure 5. Low-frequency waves upstream of the bow shock on 13 April 1998. (a) Power spectra for three mean-field magnetic field components. The local proton gyrofrequency is indicated by the vertical dashed line. The data are high pass filtered with cutoff frequency of 0.005 Hz, and the curves represent average power spectra over 1 hour. (b) A hodogram of B_X versus B_Y in principal axis (PA) coordinates for band pass filtered data. The oscillation is in a left-hand sense around the mean magnetic field.

While the frequency range of the two types of waves is similar, the waves at the flanks are more likely to be observed above the local gyrofrequency. The amplitude of the waves on the flanks is larger and more variable than near the subsolar point, and their eccentricities are slightly lower. The waves near the subsolar point propagate at a smaller angle to the background magnetic field. The differences in wave characteristics between the two locations could be explained by a difference in the source regions, by a difference in the source mechanisms, or if the waves in one region (near the subsolar point) are observed sooner after generation than the waves from another region (the flanks).

[16] Several trends are noted in the wave power. First, the wave intensity varies spatially. To demonstrate this, we took FFTs of MAG data every 30 s and extracted the power at the local proton gyrofrequency from the three mean-field magnetic field components. Figure 6 shows the power in one of the perpendicular magnetic field components as a function of location. The best fit shock location is shown in black. Inside of the shock the power is generally high in the magnetosheath (between the shock and the magnetic pile-up boundary), and it is highest at the subsolar point and in the tailward sheath. This power could be indicative of broadband turbulence or of the waves we observe upstream. Outside of the shock, power is highest in regions where there is a high concentration of waves (see Figure 4) and decreases with distance from the shock. This decrease with distance is more rapid for the upstream waves at low solar zenith angle than at high solar zenith angle. PCW intensity decreases with altitude during a given orbit.

[17] The proposed generation mechanisms for these waves involve interaction of the solar wind with the Martian hydrogen exosphere [*Russell et al.*, 1990; *Sauer et al.*, 2001]. Thus the generation of these waves likely depends upon exospheric density. We can use altitude profiles of wave intensity from each MGS orbit to derive an exospheric "scale height" at Mars using very simple assumptions. We assume that the waves are observed at their source, that wave intensity varies with altitude only according to exospheric density, and that exospheric scale height is a constant with altitude over the altitude range that we sample. Therefore, if $H(z) = H$, $n(z) = n_0 e^{-z/H}$, and $I(z) = Cn^b$, we find that $H/b = (z_2 - z_1)/\ln(I_1/I_2)$, where I_1 and I_2 are wave intensities measured at altitudes z_1 and z_2, respectively, H is "scale height," n is particle density, and C and b are constants. Each of the assumptions is problematic. We likely do not always observe the waves at their source, and we suspect that the waves observed at the flanks are convected from either the subsolar point or from the magnetosheath. We do not know that the only altitude variation of wave intensity comes from neutral particle density. However, we expect the quantity of pickup ions created from each of the three main ionization

Table 1. Upstream PCW Characteristics[a]

Upstream Waves	ω, Hz	ω/Ω_c^+	A, nT	$\delta B/B$	ϵ	θ_{kB}, deg
All waves	0.041–0.100	0.85–1.51	0.19–0.53	0.20–0.56	0.48–0.78	13.9–33.7
SPO1	0.044–0.081	0.87–1.27	0.13–0.33	0.15–0.26	0.61–0.83	10.6–22.5
AB1 "flank"	0.039–0.094	0.84–1.58	0.23–0.56	0.27–0.63	0.50–0.77	15.2–36.6

[a]Each range of values denotes the quartiles around the median value.

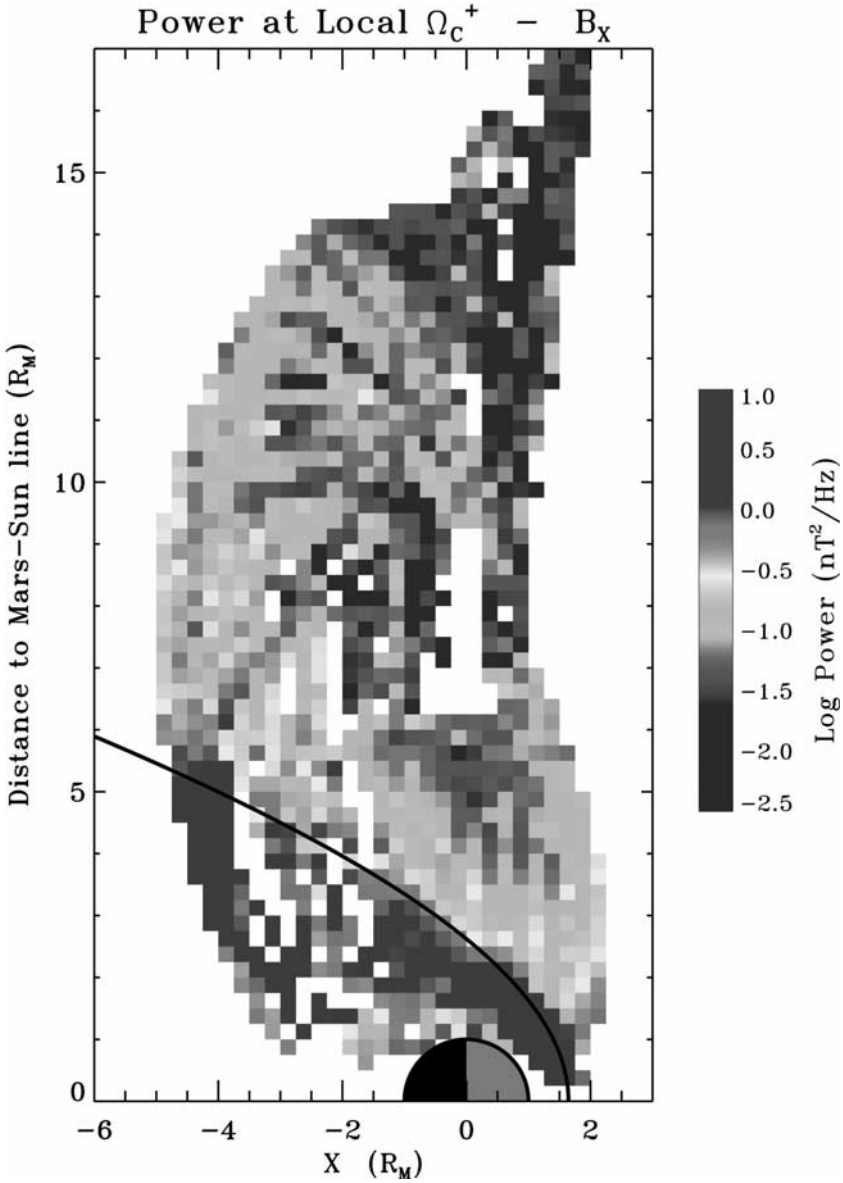

Figure 6. Spatial distribution of power at the local proton gyrofrequency. Average power is shown as a function of location for the x component of magnetic field in mean-field coordinates. The best fit bow shock is indicated in black. See color version of this figure at back of this issue.

processes of electron impact, charge exchange, and photoionization to vary linearly with exospheric density ($b = 1$). Finally, we can not be sure that the exospheric scale height does not vary with temperature; however, the exosphere is collisionless, and at the altitudes at which we observe the waves we do not expect the temperatures to vary strongly with altitude. Using each orbit of data individually, we find that H/b has a value of 3170 km ± 1480 km for SPO1 upstream data in the altitude range 5500–18,500 km, and 2070 km ± 1850 km for flank in the altitude range 15,500–45,500 km. If $b = 1$, then the exospheric scale height is ~2000–3000 km. This is much larger than the scale height for hydrogen of ~800 km inferred from *Nagy and Cravens* [1988] and *Shinigawa and Cravens* [1989] by *Crider* [1999], and much smaller than the scale height of ~16,000 km derived by *Barabash et al.* [1991]. We calculate scale height at much higher altitudes than *Crider* [1999], and we use a much simpler definition than *Barabash et al.* [1991].

[18] It is interesting to note that the two spatial concentrations of waves occur ~6–8 R_M apart. Assuming that the local magnetic field magnitude is 6 nT and that the solar wind velocity is 400 km/s, the distance that a recently picked-up exospheric particle would travel over a single gyroperiod as it is convected downstream by the solar wind is ~1.3 R_M for hydrogen, and ~21 R_M for oxygen. The PCWs at the flank, then, do not appear to be attributable to convection of the subsolar waves downstream. They are either generated locally outside of the shock, or are generated elsewhere (such as in the magneto-

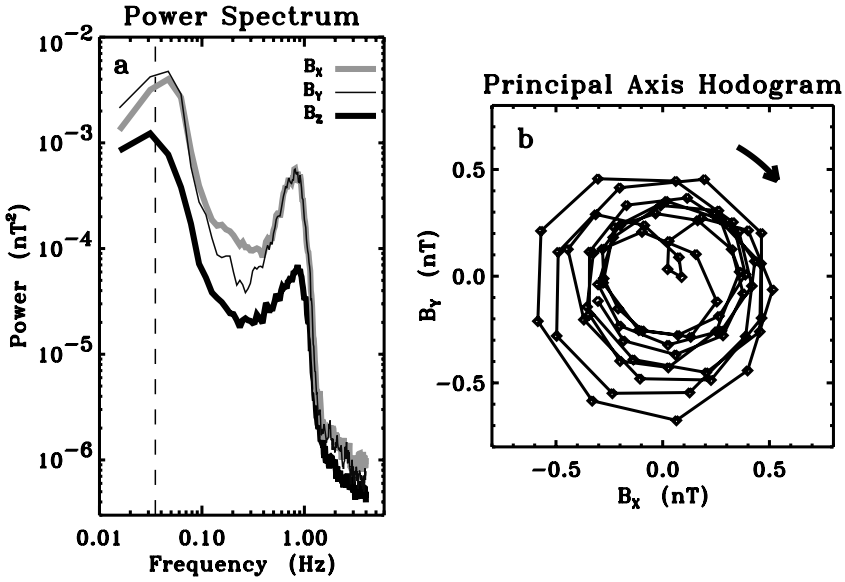

Figure 7. Whistler waves upstream of the bow shock on 11 December 1997. (a) Power spectra for three mean-field magnetic field components. The local proton gyrofrequency is indicated by the vertical dashed line. The data are high pass filtered with cutoff frequency of 0.01 Hz, and the curves represent average power spectra over 1 hour. (b) A hodogram of B_X versus B_Y in PA coordinates for band pass filtered data. The oscillation is in a left-hand sense around the mean magnetic field.

sheath) and propagate/are convected to the region where they are observed.

3.2. High-Frequency Waves

[19] At Earth and other solar system bodies, whistler waves are observed in the shock foot, in wave trains upstream from the shock, and near disturbances in the solar wind [e.g., *Fairfield*, 1974; *Heppner et al.*, 1967; *Russell et al.*, 1971]. Each of these phenomena is observed in high time resolution MGS data, and we focus here on relatively long-lived (minutes to tens of minutes) upstream whistler trains.

[20] The same technique described above for PCWs was employed to study the whistler waves. High time resolution MAG data from selected upstream time periods was band pass filtered (to exclude the local gyrofrequency and high-frequency noise) and examined every 4 s for the presence of the whistler disturbance. For each identified wave example, principal axis analysis was used to determine the peak frequency, amplitude, polarization, eccentricity, and propagation direction for the wave. The background magnetic field direction (calculated from low time resolution data) was used to determine whether MGS was in the foreshock (magnetically connected to the bow shock). For those observations connected to the bow shock, the distance to the shock along the field line was recorded.

[21] Figure 7 shows power spectra for all three magnetic field components in mean-field coordinates on 11 December 1997. FFTs were constructed from MAG data every 16 s over a 60 min time span and averaged together to create the displayed power spectra. PCWs are seen at the local proton gyrofrequency (indicated by the dashed line) for this orbit, and the whistler waves are evident near 1 Hz. The whistler wave power is mostly transverse, and the wave propagates at ($\sim$16°) to the background magnetic field. A hodogram of 10 s of data in PA coordinates from this time period is shown in Figure 7b. The wave oscillates around the mean magnetic field (out of the page) in a left-hand sense. Not all examples of the whistler waves propagate at such a small angle to the background field, and not all examples are left-hand polarized. Left-hand spectra typically have a sharp peak and a steep falloff at high frequencies. Right-hand spectra do not have a sharp peak.

[22] Important features of upstream whistlers at other planets include an association with the foreshock, a correlation between the sense of polarization and the angle the solar wind flow makes with the magnetic field (or wave propagation vector), and a decrease of wave amplitude with distance to the shock along the magnetic field line [*Orlowski and Russell*, 1995]. Each of these distinguishing characteristic is observed for the waves at Mars. Of the observations determined to contain whistler waves, 88% occurred while MGS was magnetically connected to the bow shock. The remaining 12% could be attributable to uncertainty in determination by MAG of the mean-field direction, or to upstream disturbances that can cause whistlers, such as hot diamagnetic cavities [*Øieroset et al.*, 2001].

[23] Figure 8 shows that the sense of polarization is controlled by the direction of the solar wind flow with respect to the magnetic field. The figure shows the frequency of whistler waves as a function of the angle between the magnetic field direction (determined from low time resolution data) and solar wind velocity (taken in the x direction for lack of better solar wind velocity information). Negative frequencies indicate left-hand polarization in the rest frame of MGS. When the magnetic field is at a high angle to the flow, the sense of polarization of the waves is right-handed. Below $\sim$66° the polarization sense is left-handed. This trend is observed because of the relative

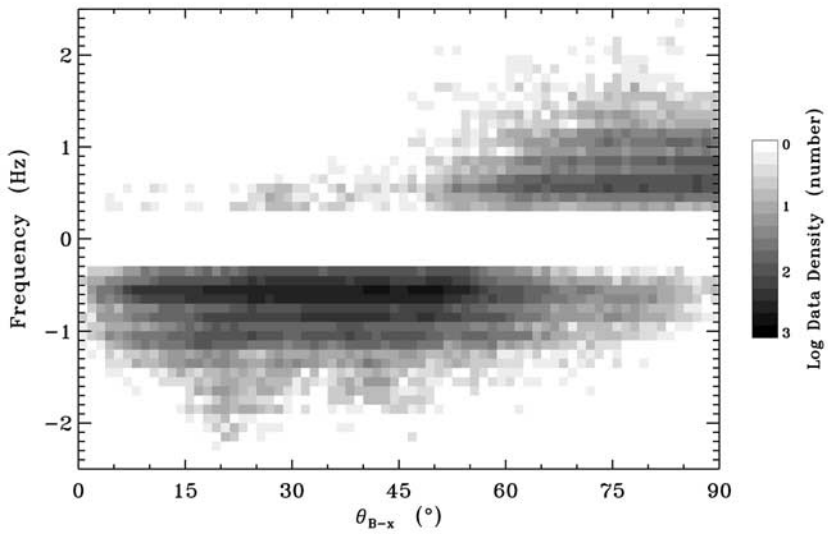

Figure 8. Frequency of the whistler waves as a function of the angle between the magnetic field and the solar wind velocity. The solar wind velocity is taken in the *x* direction. Negative frequencies indicate left-hand polarization in the rest frame of MGS.

motion between the solar wind flow and the spacecraft. As pointed out by *Fairfield* [1974], the whistler waves are right-handed in the rest frame of the plasma, and they are able to propagate upstream from the shock because their group velocity is greater than the solar wind velocity of ~400 km/s. However, the wave can appear to be left-handed in the rest frame of the spacecraft because the component of the wave's group velocity in the same direction as the solar wind flow is Doppler shifted. The larger the angle between the wave propagation vector and the solar wind velocity vector, the smaller the observed Doppler shift. The waves propagate obliquely to the magnetic field; therefore, the larger the angle between the IMF direction and the solar wind, the more likely the waves are to be observed with their intrinsic right-handed polarization. No waves are indicated at low frequency in Figure 8 because frequencies near the local proton gyrofrequency were excluded from this analysis. The striped effect in the figure arises because MAG data have discrete time resolution; thus the frequency resolution of FFTs of MAG data is also discrete.

[24] The decrease in wave intensity with distance from the shock is demonstrated for Mars in Figure 9. The path length from the spacecraft location to the shock along the field line was calculated for each whistler wave observation. Overall, the median wave amplitude for waves with peak frequency between 0.3 and 1.3 Hz decreases from the shock out to ~8 R_M. Beyond that distance the amplitude of the waves becomes too low to be distinguished in MAG data, and the observed wave amplitude levels off. That damping of upstream whistlers is believed to be governed by details

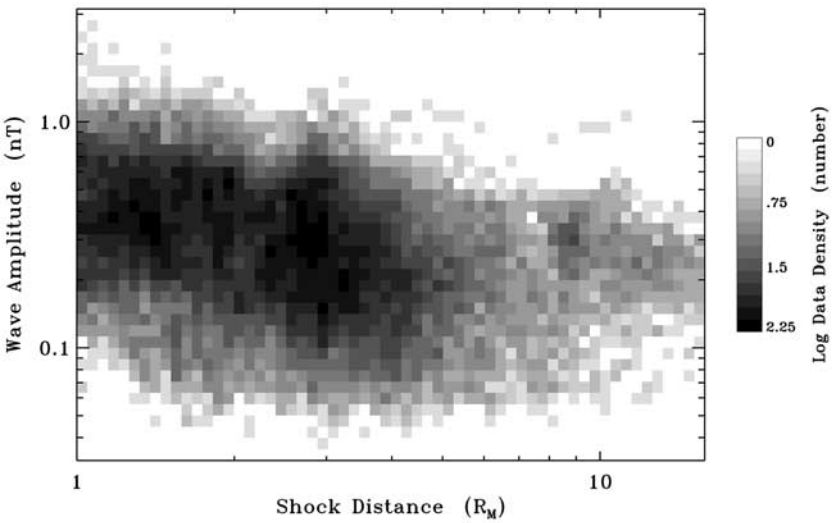

Figure 9. Wave amplitude as a function of distance to the shock along the magnetic field line for waves with peak frequency between 0.3 Hz and 1.3 Hz.

Table 2. Upstream Whistler Waves in the Solar System[a]

Planet	ω, Hz	*A*, nT	ϵ	θ_{kB}, deg	θ_{kx}, deg
Mercury[b]	2.5–3.0	0.2–3.2	0.2–0.65	7–53	0–37
Venus[b]	1.0–1.8	0.3–1.9	0.75–0.99	5–51	830
Earth[b]	0.8–1.5	0.1–0.6	0.71–0.9	5–57	9–36
Mars	0.5–0.8	0.2–0.5	0.73–0.89	19–40	21–38
Saturn[b]	0.1–0.2	0.01–0.04	0.6	40–60	60–70

[a]Each range of values for Mars denotes the quartiles around the median value.
[b]Source is *Orlowski and Russell* [1995]. (Reprinted with permission from the Committee on Space Research.)

of the electron distribution; the spread in wave amplitudes at a given distance from the shock may be attributed to the local electron population. Whistler waves observed closer to the shock (<1 R_M) had even higher amplitudes than those shown in Figure 9, but they are likely from the shock foot whistlers studied by *Fairfield* [1974] and not from upstream whistler wave trains.

[25] It is certain that the observed upstream waves are the whistlers reported for other solar system bodies. A comparative study of these whistlers at other bodies have noted trends in the wave characteristics with the distance of the body from the Sun [*Orlowski and Russell*, 1995]. For the first time, we are able to put Martian whistler waves in context with other planets. The results are summarized in Table 2. For Mars the quartile values around the median are given for each quantity. Martian waves follow the trends observed at other planets. The frequency of the waves in the frame of the spacecraft decreases with heliocentric distance. The waves are thought to be generated at broad range of frequencies (25–100 Ω_C^+) in the plasma frame, and the frequency difference between the planets reflects the difference in Doppler shift with increasing heliocentric distance (and increasing solar wind spiral angle). Eccentricity increases and amplitude decreases with heliocentric distance. The whistler waves propagate at a moderate angle to the background magnetic field. The angle between the wave propagation vector and the flow velocity increases with distance as the solar wind magnetic field becomes less radial. Whistlers are most likely generated in the shock foot and propagate upstream in the foreshock at each of these bodies [*Orlowski and Russell*, 1995]; the fact that wave characteristics vary smoothly with heliocentric distance suggests that similar processes must act at each body to produce these waves. At the same time, the observed trends with heliocentric distance suggest that the solar wind interaction with the shock or foreshock of each body results in different wave characteristics at each planet.

4. Conclusions

[26] MGS MAG records perturbations to the magnetic field upstream from the Martian shock that result from electromagnetic plasma wave propagation. Two wave modes were examined in MAG data: a wave observed at the local proton gyrofrequency and higher-frequency whistler waves.

[27] For waves at the local gyrofrequency, the main results of this analysis are as follows:

1. The spatial distribution of the waves with respect to Mars is determined to be concentrated near the subsolar point and near the flanks of the solar wind interaction. There is a paucity of waves observed near the Martian terminator plane. These PCWs are more powerful at low altitude than at high altitude. The waves are also present in the magnetosheath.

2. Hundreds of orbits of data were analyzed to determine the characteristics of the waves. The frequency (near the local gyrofrequency), eccentricity (~0.60), and propagation angle ($\theta_{\mathbf{kB}}$) agree with those determined from Phobos observations, while the wave amplitude is 2–3 times higher than observed by Phobos.

3. Waves observed near the subsolar point differ from the waves observed near the flanks. The subsolar waves are more circular, have lower amplitude, propagate at a smaller angle to the magnetic field, and their intensity falls off less rapidly with altitude than the waves on the flanks.

4. The observed wave features (left-hand polarization, decreasing amplitude with altitude, spatial distribution) are consistent with solar wind pickup of Mars' hydrogen exosphere.

[28] For whistler waves, the main results of this analysis are as follows:

1. Upstream whistler waves in the frequency range 0.4–2.3 Hz are reported at Mars for the first time from magnetometer data.

2. Wave characteristics are consistent with observations at other solar system bodies (summarized by *Orlowski and Russell* [1995]) and follow the trends with heliocentric distance observed at other bodies. Specifically, the frequency and amplitude of the waves decrease with heliocentric distance, while the angle between **k** and the solar wind flow direction increases. The whistler waves propagate obliquely to the magnetic field.

3. The similarities between waves observed at Mars and at other solar system bodies suggest that similar processes are at work at the shocks and in the foreshocks of those bodies that result in the generation and propagation of upstream whistlers.

[29] Future work on upstream plasma waves at Mars should focus on the generation mechanisms for the two waves studied here. MGS does not have a solar wind plasma instrument, and observations of LF waves at the proton cyclotron frequency throughout the Martian system need to be made in conjunction with solar wind plasma and velocity measurements, as well as exospheric density measurements. The differences between subsolar waves and flank waves should be explored to discover whether the waves observed on the flanks have been convected from the subsolar region, convected/propagated from the Martian sheath, or are generated locally. If formed locally, they could be generated by a similar mechanism to the mechanism that operates in the subsolar region, or by a different mechanism. Exospheric measurements can be used to determine the chief ionization process for the particles causing the waves.

[30] There is much that is still not understood about the upstream whistlers. It is believed that the electron distribution function plays an important role in the damping and evolution of these waves [*Orlowski et al.*, 1995], but several authors have not ruled out the role of protons in whistler wave formation [*Hellinger and Mangeney*, 1997; *Balikhin et al.*, 1999]. A study of simultaneous magnetic field and particle observations (from MGS or from future spacecraft)

may reveal how the electron distribution function affects these waves and whether protons are capable of causing some of the observed whistlers. Simultaneous plasma measurements of the wave and the solar wind velocity are critical for constraining details of the wave propagation and can be used to estimate the thickness of the Martian shock and the frequency of the waves in the plasma frame.

[31] The NOZOMI spacecraft is equipped with a suite of plasma instruments including a magnetometer, electron temperature probe, electron and ion spectrometers, and neutral mass spectrometer. The two plasma wave analyzers on NOZOMI are designed to detect plasma waves at frequencies above 10 Hz, which is higher than the observed frequency range for either of the waves studied here. Therefore time series analysis of magnetometer data will be essential for detecting these waves. It is hoped that future analysis of MGS data and results from future spacecraft such as NOZOMI will shed light on the outstanding questions for both waves mentioned above.

[32] **Acknowledgments.** The authors thank the reviewers for their detailed and thoughtful critique.

[33] Janet G. Luhmann thanks Christopher T. Russell and another referee for their assistance in evaluating this manuscript.

References

Acuña, M. H., et al., Magnetic field and plasma observations at Mars: Initial results from the Mars Global Surveyor Mission, *Science*, *279*, 1676–1680, 1998.

Acuña, M. H., et al., Magnetic field of Mars: Summary of results from the aerobraking and mapping orbits, *J. Geophys. Res.*, *106,* 23,403–23,417, 2001.

Albee, A. L., Mars 2000, *Annu. Rev. Earth Planet. Sci.*, *28*, 281–304, 2000.

Balikhin, M. A., H. St-C. K. Alleyne, R. A. Treumann, M. N. Nozdrachev, S. N. Walker, and W. Baumjohann, The role of nonlinear interaction in the formation of LF whistler turbulence upstream of a quasi-perpendicular shock, *J. Geophys. Res.*, *104*, 12,525–12,535, 1999.

Barabash, S., and R. Lundin, Reflected ions near Mars: Phobos-2 observations, *Geophys. Res. Lett.*, *20*, 787–790, 1993.

Barabash, S., E. Dubinin, N. Pissarenko, R. Lundin, and C. T. Russell, Picked-up protons near Mars: Phobos observations, *Geophys. Res. Lett.*, *18*, 1805–1808, 1991.

Baumgärtel, K., and K. Sauer, Support for the shock source hypothesis of upstream whistlers from Hall-MHD calculations, *Adv. Space Res.*, *15*, 93–96, 1995.

Brain, D. A., M. H. Acuña, J. E. P. Connerney, F. Bagenal, D. Mitchell, D. H. Crider, and P. A. Cloutier, Observation of ion cyclotron waves with MGS MAG/ER (abstract), *Eos Trans. AGU*, 79(45), Fall Meet. Suppl., F530, 1998.

Brinca, A. L., Cometary linear instabilities: From profusion to perspective, in *Cometary Plasma Processes, Geophys. Monogr. Ser.*, vol. 61, edited by A. D. Johnstone, pp. 211–221, AGU, Washington, D. C., 1991.

Cloutier, P. A., Venus-like interaction of the solar wind with Mars, *Geophys. Res. Lett.*, *26*, 2685–2688, 1999.

Crider, D. H., Evidence of electron impact ionization in the magnetic pileup boundary of Mars—Observations and modeling results, Ph.D. thesis, 109 pp., Rice Univ., Houston, Tex., May 1999.

Fairfield, D. H., Whistler waves observed upstream from collisionless shocks, *J. Geophys. Res.*, *79*, 1368–1378, 1974.

Gary, S. P., Electromagnetic ion/ion instabilities and their consequences in space plasmas: A review, *Space Sci. Rev.*, *56*, 373–415, 1991.

Grard, R., A. Pedersen, S. Klimov, S. Savin, A. Skalsky, J. G. Trotignon, and C. Kennel, First measurements of plasma waves near Mars, *Nature*, *341*, 607–609, 1989.

Hellinger, P., and A. Mangeney, Upstream whistlers generated by protons reflected from a quasi-perpendicular shock, *J. Geophys. Res.*, *102*, 9809–9819, 1997.

Heppner, J. P., M. Sugiura, T. L. Skillman, B. G. Ledley, and M. Campbell, OGO-A magnetic field observations, *J. Geophys. Res.*, *72*, 5417–5471, 1967.

Hoppe, M. M., C. T. Russell, L. A. Frank, T. E. Eastman, and E. W. Greenstadt, Upstream hydromagnetic waves and their association with backstreaming ion populations: ISEE 1 and 2 observations, *J. Geophys. Res.*, *86*, 4471–4492, 1981.

Hoppe, M. M., C. T. Russell, T. E. Eastman, and L. A. Frank, Characteristics of the ULF waves associated with upstream ion beams, *J. Geophys. Res.*, *87*, 643–650, 1982.

Mace, R. L., Whistler instability enhanced by suprathermal electrons within the Earth's foreshock, *J. Geophys. Res.*, *103*, 14,643–14,654, 1998.

Mazelle, C., and F. M. Neubauer, Discrete wave packets at the proton cyclotron frequency at comet P/Halley, *Geophys. Res. Lett.*, *20*, 153–156, 1993.

Mazelle, C., et al., Nonlinear low frequency waves observations by Mars Global Surveyor (abstract), *Eos Trans. AGU*, *81*(48), Fall Meet. Suppl., F964, Abstract SH61A-05, 2000.

Nagy, A. F., and T. E. Cravens, Hot oxygen in the upper atmospheres of Venus and Mars, *Geophys. Res. Lett.*, *15*, 433–435, 1988.

Øieroset, M., D. L. Mitchell, T. D. Phan, and R. P. Lin, Hot diamagnetic cavities upstream of the Martian bow shock, *Geophys. Res. Lett.*, *28*, 887–890, 2001.

Orlowski, D. S., and C. T. Russell, Comparison of properties of upstream whistlers at different planets, *Adv. Space Res.*, *15*, 37–41, 1995.

Orlowski, D. S., G. K. Crawford, and C. T. Russell, Upstream waves at Mercury, Venus and Earth: Comparison of the properties of one Hertz waves, *Geophys. Res. Lett.*, *341*, 2293–2296, 1990.

Orlowski, D. S., C. T. Russell, and R. P. Lepping, Wave phenomena in the upstream region of Saturn, *J. Geophys. Res.*, *97*, 19,187–19,199, 1992.

Orlowski, D. S., C. T. Russell, D. Krauss-Varban, N. Omidi, and M. F. Thomsen, Damping and spectral formation of upstream whistlers, *J. Geophys. Res.*, *100*, 17,117–17,128, 1995.

Riedler, W., et al., Magnetic fields near Mars: First results, *Nature*, *341*, 604–607, 1989.

Russell, C. T., D. D. Childers, and P. J. Coleman Jr., Ogo 5 observations of upstream waves in the interplanetary medium: Discrete wave packets, *J. Geophys. Res.*, *76*, 845–861, 1971.

Russell, C. T., J. G. Luhmann, K. Schwingenschuh, W. Riedler, and Y. Yeroshenko, Upstream waves at Mars: Phobos observations, *Geophys. Res. Lett.*, *17*, 897–900, 1990.

Russell, C. T., J. G. Luhmann, K. Schwingenschuh, W. Riedler, and Y. Yeroshenko, Upstream waves at Mars, *Adv. Space Res.*, *12*, 251–254, 1992.

Sagdeev, R. Z., V. D. Shapiro, V. I. Shevchenko, A. Zaiharov, P. Kiraly, K. Szego, A. F. Nagy, and R. J. Grard, Wave activity in the neighborhood of the bow shock of Mars, *Geophys. Res. Lett.*, *17*, 893–896, 1990.

Sauer, K., E. Dubinin, and J. F. McKenzie, New type of soliton in bi-ion plasmas and possible implications, *Geophys. Res. Lett.*, *28*, 3589–3592, 2001.

Sentman, D. D., M. F. Thomsen, S. P. Gary, W. C. Feldman, and M. M. Hoppe, The oblique whistler instability in the Earth's foreshock, *J. Geophys. Res.*, *88*, 2048–2056, 1983.

Shinigawa, H., and T. E. Cravens, A one-dimensional multispecies magnetohydrodynamic model of the dayside ionosphere of Mars, *J. Geophys. Res.*, *94*, 6506–6516, 1989.

Song, P., and C. T. Russell, Time series data analyses in space physics, *Space Sci. Rev.*, *87*, 387–463, 1999.

Tsurutani, B. T., Comets: A laboratory for plasma waves and instabilities, in *Cometary Plasma Processes, Geophys. Monogr. Ser.*, vol. 61, edited by A. D. Johnstone, pp. 189–209, AGU, Washington, D. C., 1991.

Vignes, D., C. Mazelle, H. Reme, M. H. Acuña, J. E. P. Connerney, R. P. Lin, D. L. Mitchell, P. Cloutier, D. H. Crider, and N. F. Ness, The solar wind interaction with Mars: Locations and shapes of the bow shock and magnetic pile-up boundary from the observations of the MAG/ER experiment onboard Mars Global Surveyor, *Geophys. Res. Lett.*, *27*, 49–52, 2000.

Wong, H. K., and C. W. Smith, Electron beam excitation of upstream waves in the whistler mode frequency range, *J. Geophys. Res.*, *99*, 13,373–13,387, 1994.

M. H. Acuña, J. E. P. Connerney, and D. H. Crider, NASA Goddard Space Flight Center, Code 695.0, Greenbelt, MD 20701, USA. (mario.acuna@gsfc.nasa.gov; john.connerney@gsfc.nasa.gov; dana.crider@gsfc.nasa.gov)

F. Bagenal and D. A. Brain, Laboratory for Atmospheric and Space Physics, University of Colorado, Campus Box 392, Boulder, CO 80309, USA. (bagenal@lasp.colorado.edu; david.brain@colorado.edu)

C. Mazelle, CESR, 9, Avenue du colonel Roche, BP 4346, F-31028, Toulouse, France. (christian.mazelle@cesr.fr)

D. L. Mitchell, Space Sciences Laboratory, University of California, Berkeley, CA 94720-7450, USA. (mitchell@ssl.berkeley.edu)

N. F. Ness, Bartol Research Institute, University of Delaware, 217 Sharp Lab, Newark, DE 19716, USA. (nfness@bartol.udel.edu)

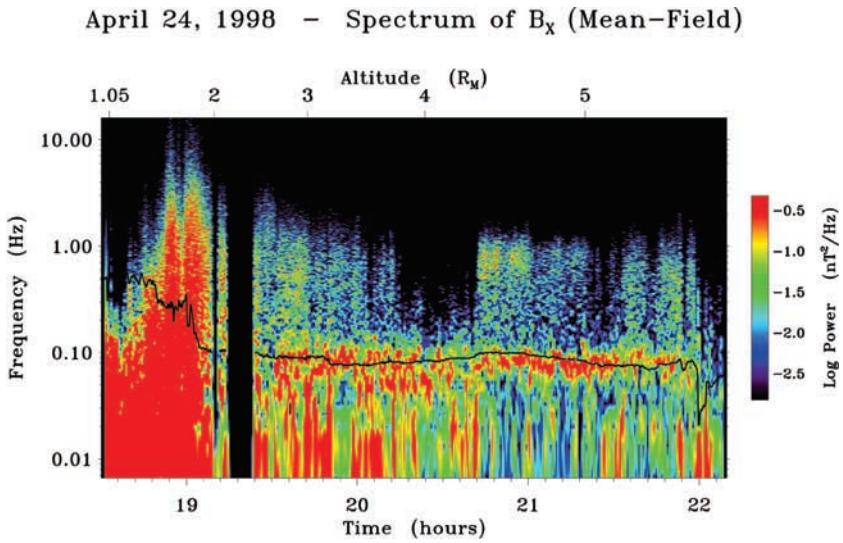

Figure 3. Spectrogram of power as a function of frequency and time for the B_X field component in mean-field coordinates for 24 April 1998. The bow shock crossing occurs at ∼1910 UT, after which MGS is outside of the shock for this SPO1 orbit. Low-frequency waves occur near the local proton gyrofrequency (plotted over the spectrogram in black), and high-frequency waves occur near 1 Hz. There are two data gaps between 1906 and 1924 UT.

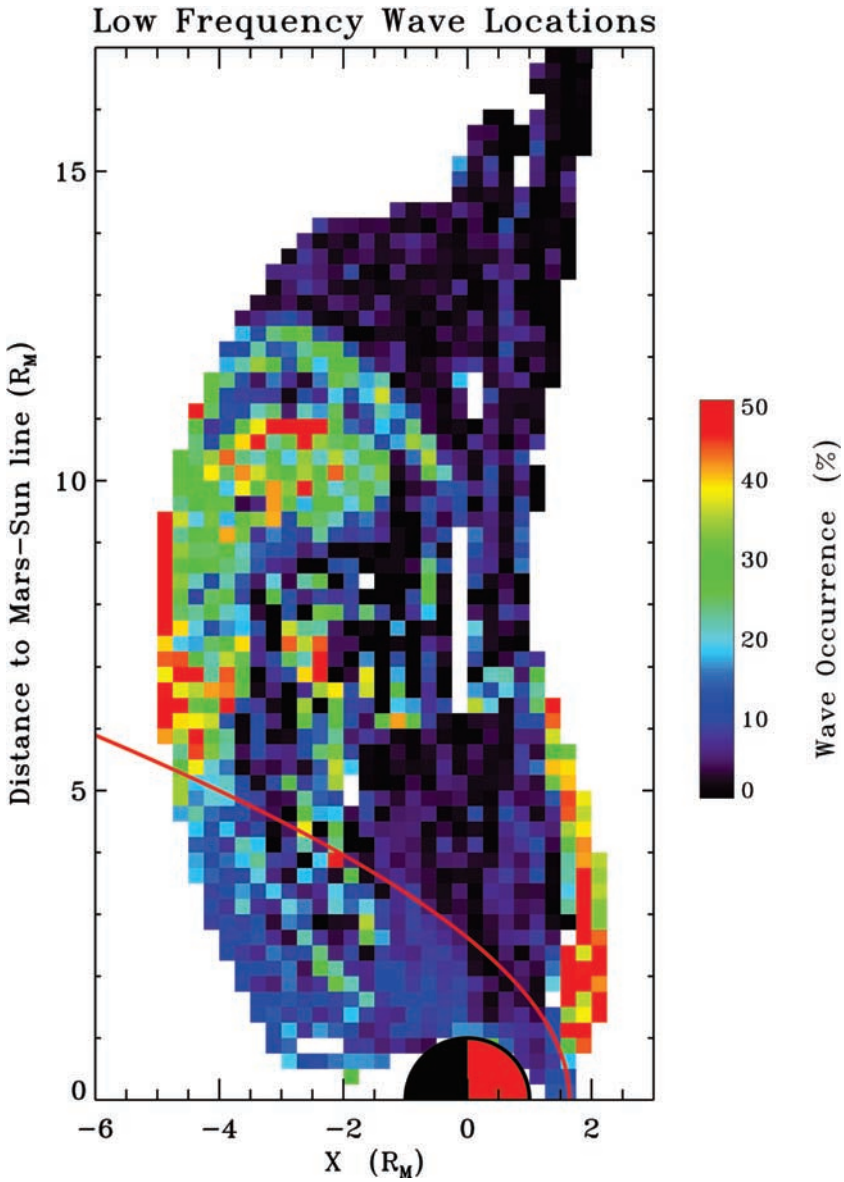

Figure 4. Spatial distribution of waves detected at the local proton gyrofrequency. The percentage of observations that were determined to contain waves is shown for each spatial bin. The best fit bow shock is indicated in red.

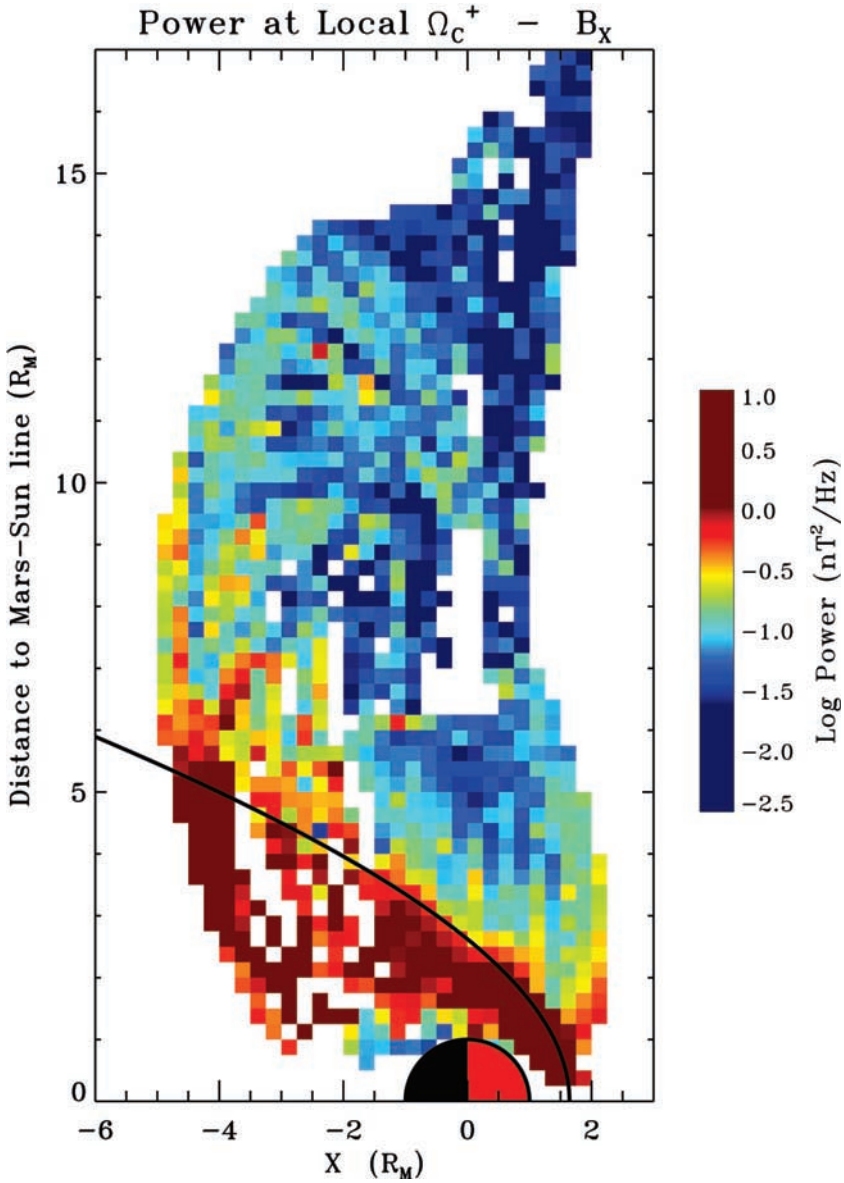

Figure 6. Spatial distribution of power at the local proton gyrofrequency. Average power is shown as a function of location for the *x* component of magnetic field in mean-field coordinates. The best fit bow shock is indicated in black.